



ORIGIN OF CHAOS IN A TWO-DIMENSIONAL MAP MODELING SPIKING-BURSTING NEURAL ACTIVITY

ANDREY L. SHILNIKOV

*Department of Mathematics and Statistics,
Georgia State University, Atlanta, GA 30303-3083, USA*

NIKOLAI F. RULKOV

*Institute for Nonlinear Science,
University of California at San Diego, La Jolla, CA 92093, USA*

Received August 22, 2002; Revised September 20, 2002

Origin of chaos in a simple two-dimensional map model replicating the spiking and spiking-bursting activity of real biological neurons is studied. The map contains one fast and one slow variable. Individual dynamics of a fast subsystem of the map is characterized by two types of possible attractors: stable fixed point (replicating silence) and superstable limit cycle (replicating spikes). Coupling this subsystem with the slow subsystem leads to the generation of periodic or chaotic spiking-bursting behavior. We study the bifurcation scenarios which reveal the dynamical mechanisms that lead to chaos at alternating silence and spiking phases.

Keywords: Chaos; canards; maps; spiking-bursting oscillations; neurons.

1. Introduction

Spiking-bursting activity of biological neurons is the result of high-dimensional dynamics of nonlinear processes responsible for generation and interaction of various ionic currents flowing through the membrane channels [Hodgkin & Huxley, 1952]. Numerical studies of such neural activity are usually based on either realistic channel-based models or phenomenological models. The channel-based models proposed for a single neuron are designed to capture the physiological processes in the membrane. These models are usually given by a system of many nonlinear differential equations (see, e.g. [Hodgkin & Huxley, 1952; Chay, 1985, 1990; Chay *et al.*, 1995; Buchholtz *et al.*, 1992; Golomb *et al.*, 1993] and the review of the models in [Abarbanel *et al.*, 1996]). The phenomenological models are designed to replicate the characteristic features of the bursting behavior without direct

relation to the physiological processes in the membrane [Hindmarsh & Rose, 1984; Rinzel, 1985, 1987; Wang, 1993]. The goal of such models is to capture the most important features of neural behavior with minimal complexity of the model. It was shown that the replication of main dynamical regimes of regular and chaotic spiking-bursting neural activity can be achieved using at least a three-dimensional system of ODEs [Hindmarsh & Rose, 1984; Rinzel, 1985, 1987; Wang, 1993; Belykh *et al.*, 2000; Izhikevich, 2000].

Recently a similar type of phenomenological models, but based on a low-dimensional map, was proposed. The interest in the map models is motivated by the studies of nonlinear mechanisms behind the restructuring of the collective neural behavior in large networks. Here we consider a map model which is built following the principles for constructing a low-dimensional system of differential equations which is capable of generating

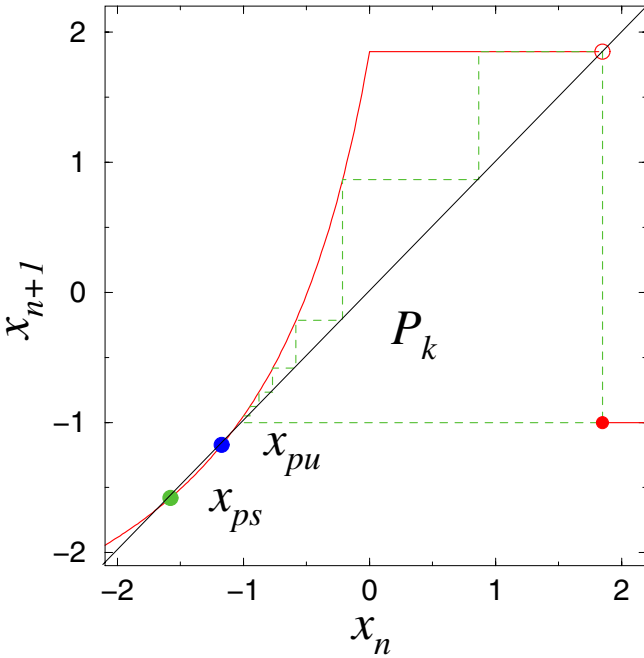


Fig. 1. Dynamics of fast map (1a) computed with $\alpha = 5.6$ and fixed value of $y_n = y = -3.75$. The shape of the non-linear function $f(x, y)$ is shown with a red line. Red circle on the diagonal indicates that this point of $f(x, y)$ does not belong to the diagonal. The dashed green line illustrates a super-stable cycle P_k . The stable and unstable fixed points of the map are indicated by x_{ps} and x_{pu} , respectively.

fast spikes bursts excited on top of the slow oscillations (see e.g. [Hindmarsh & Rose, 1984; Wang, 1993; Rinzel, 1985, 1987; Belykh *et al.*, 2000; Izhikevich, 2000]). These two time-scale oscillations are captured using a system with both slow and fast dynamics. In the case of a map, such a system can be designed in the following form [Rulkov, 2002]

$$x_{n+1} = f(x_n, y_n), \tag{1a}$$

$$y_{n+1} = y_n - \mu(x_n + 1) + \mu\sigma, \tag{1b}$$

where x_n is the fast and y_n is the slow dynamical variable. Slow time evolution of y_n is due to small values of the parameter $\mu = 0.001$. The parameter σ is a control parameter which is used to select the regime of individual behavior.

The fast map (1a) is built to mimic spiking and silent regimes. This is achieved with the use of discontinuous function $f(x, y)$ of the following form

$$f(x, y) = \begin{cases} \alpha/(1-x) + y, & x \leq 0 \\ \alpha + y, & 0 < x < \alpha + y \\ -1, & x \geq \alpha + y \end{cases} \tag{2}$$

where α is a control parameter of the map. Figure 1 shows the dependence of $f(x, y)$ on x

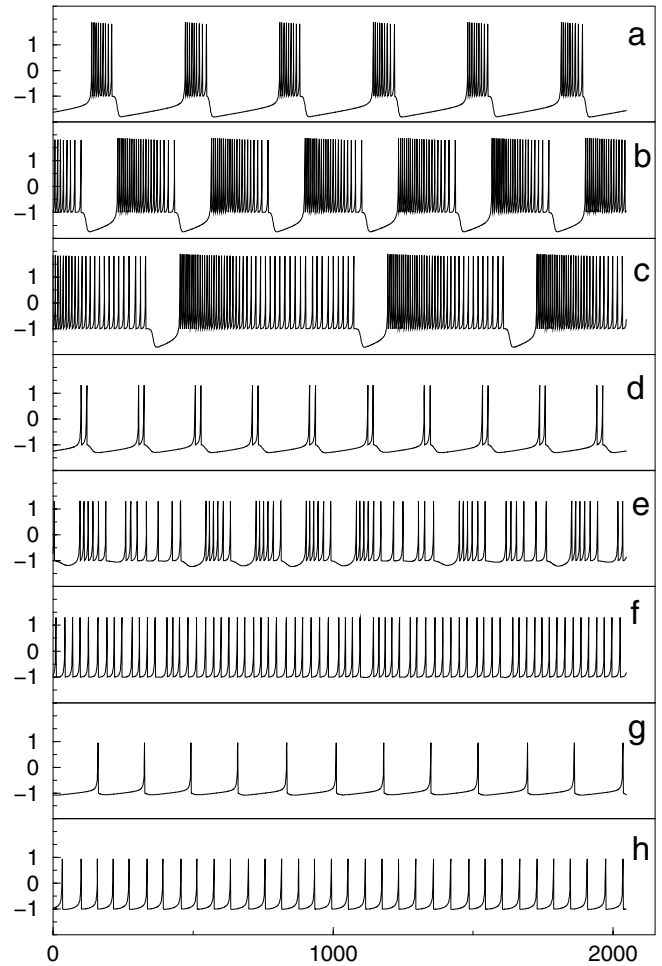


Fig. 2. Typical waveforms of spiking and spiking-bursting behavior generated by the map (1) computed for the following parameter values: (a) $\alpha = 5.6, \sigma = -0.25$; (b) $\alpha = 5.6, \sigma = 0.2$; (c) $\alpha = 5.6, \sigma = 0.322$; (d) $\alpha = 4.6, \sigma = -0.1$; (e) $\alpha = 4.6, \sigma = 0.16$; (f) $\alpha = 4.6, \sigma = 0.225$; (g) $\alpha = 3.9, \sigma = 0.04$; (h) $\alpha = 3.9, \sigma = 0.15$. The points of the consecutive iterations x_n are connected with straight lines.

computed for a fixed value of y . In this plot the values of α and y are set to illustrate the possibility of coexistence of limit cycle, P_k , corresponding to spiking oscillations in (1a), and fixed points x_{ps} and x_{pu} . The function is designed in such a way that when y increases or decreases the graph of $f(x, y)$ moves up or down, respectively, except for the third interval $x \geq \alpha + y$, where the values of $f(x, y)$ always remain equal to -1 .

Typical regimes of temporal behavior of the two-dimensional map are shown in Fig. 2. When the value of α is less than 4.0 then, depending on the value of parameter σ , the map generates spikes or stays in a steady state. The frequency of the spikes increases as the value of parameter σ is increased [see Figs. 2(g) and 2(h)].

For $\alpha > 4$ the map dynamics are capable of producing bursts of spikes. The spiking-bursting regimes are found in the intermediate region of the values of σ between the regimes of continuous tonic spiking and steady state (silence). The spiking-bursting regimes include both periodic and chaotic bursting. A few typical bursting-spiking regimes computed for different values of parameters are presented in Fig. 2(a)–2(e). Regimes of chaotic behavior are illustrated in Figs. 2(c), 2(e), and 2(f).

It was shown in [Rulkov, 2002] that using approximate analysis of fast and slow dynamics one can explain the regimes of silence, continuous spiking, and the generation of the bursts of spikes that occurred in the map (1). However such analysis does not explain the dynamical mechanism behind the chaotic spiking and chaotic spiking-bursting behaviors. Understanding of the origin of a chaotic behavior in the map is the goal of this paper.

The paper is organized as follows: Section 2 briefly outlines the results of [Rulkov, 2002] to illustrate the features of the fast and slow dynamics of the map. These results also introduce important and critical parameters of the map with $\mu \rightarrow 0$, and make this paper self-contained. Section 3.1 discusses local bifurcations of fixed point in map (1) with finite values of small parameter μ . Section 3.2 presents study of the chaotic behavior in the two-dimensional dynamics that occurs around the border of silence — spiking transition. Section 3.3 focuses on the issues of chaos origin near the critical values of parameters where continuous spiking switches to the spiking-bursting activity.

2. Fast and Slow Dynamics of the Map ($\mu \rightarrow 0$)

Due to small values of μ the mechanisms behind the bursts generation can be analyzed by splitting the system into fast and slow motions. In this approximation, time evolution of the fast variable, x , is studied with the one-dimensional map (1a) where the slow variable, y , is treated as a control parameter whose value drifts slowly in accordance with Eq. (1b). One can see from (1b) that the value of y remains unchanged only if $x = x_s$ given by

$$x_s = -1 + \sigma.$$

If $x < x_s$, then the value of y slowly increases. If $x > x_s$, then y decreases.

The fixed points x_p of the fast map (1a) define the branches of slow motions in the two-dimensional

phase space (x_n, y_n) . They are given by the equation of the form

$$y = x_p - \frac{\alpha}{1 - x_p}, \quad (3)$$

where $x_p \leq 0$. The stable branch $S_{ps}(y)$ exists for $x_p < 1 - \sqrt{\alpha}$ and the unstable branch $S_{pu}(y)$ exists within $1 - \sqrt{\alpha} \leq x_p \leq 0$. Considering the fast and slow dynamics together, one can see that the point of intersection of line $x = x_s$ with these branches defines a fixed point of the two-dimensional map (1). This point is called Operating Point (OP).

The stable OP corresponds to the regime of silence in the neural dynamics. The oscillations in the map dynamics appear when OP becomes unstable. In the limit $\mu \rightarrow 0$, the threshold of excitation σ_{th} is given by equation

$$\sigma_{th} = 2 - \sqrt{\alpha}. \quad (4)$$

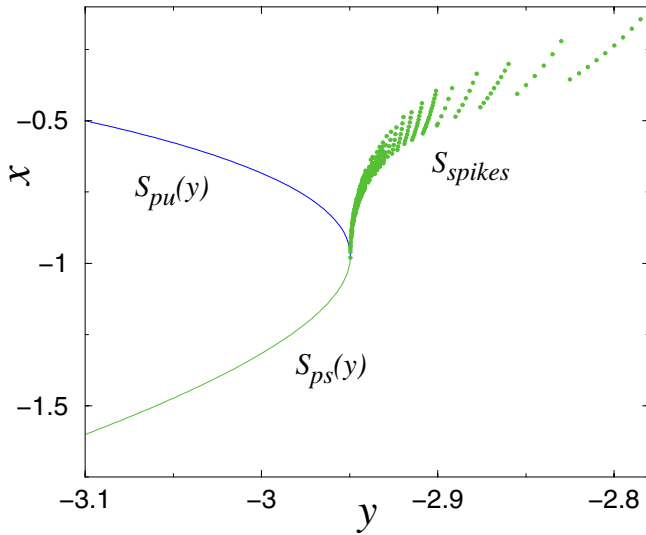
To obtain a complete picture of the fast–slow dynamics we need to consider the branch of spiking regime. For small μ the location of this branch, can be approximated by mean values of x_n computed for periodic trajectory P_k of the fast map (1a) with fixed values of y

$$x_{\text{mean}} = \frac{1}{k} \sum_{m=1}^k f^{(m)}(-1, y), \quad (5)$$

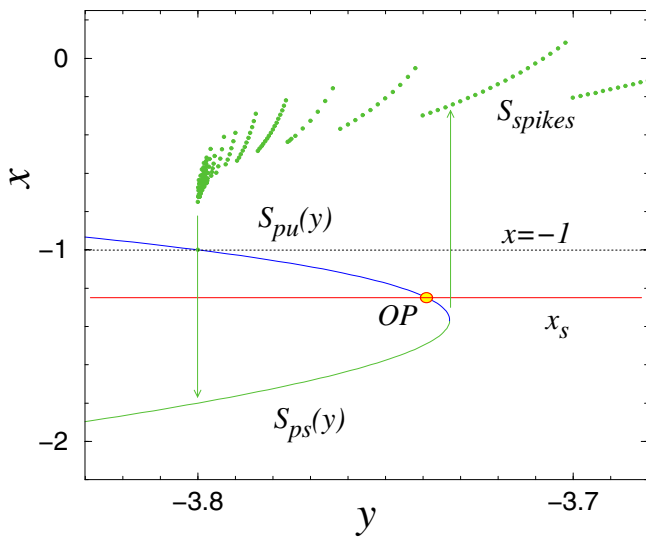
where k is the period of P_k , and $f^{(m)}(x, y)$ is the m th iterate of (1a), starting at point x . The spiking branch of “slow” dynamics S_{spikes} is shown in Fig. 3. One can see that this branch has discontinuities caused by the sequence of bifurcations of cycle P_k which monotonously change the value of k .

For the parameter values $\alpha > 4$, it is important to take into account the formation of homoclinic orbit h_{pu} in fast map (1a). This homoclinic orbit originates from the unstable fixed point, x_{pu} , and occurs when the coordinate of x_{pu} becomes equal to -1 . The homoclinic orbit forms at the value of y where the unstable branch $S_{pu}(y)$ crosses the line $x = -1$, see Fig. 3(b). When map (1) is firing spikes and the value of y gets to the bifurcation point, the cycle P_k merges into the homoclinic orbit, disappears, and then the trajectory of the map jumps to the stable fixed point x_{ps} .

Typical phase portraits of the model, obtained under the assumptions made above, are presented in Fig. 3. Figure 3(a) illustrates the case when $2 < \alpha \leq 4$. The dynamical mechanism resulting in spiking-bursting oscillation is shown in Fig. 3(b).



(a)



(b)

Fig. 3. Stable ($S_{ps}(y)$, S_{spikes} shown by green) and unstable ($S_{pu}(y)$ shown by blue) branches of slow dynamics of (1) plotted on the plane of phase variables (y, x). The cases of $\alpha = 3.9$ and $\alpha = 5.6$ are presented in (a) and (b), respectively. The operating point OP in (b) is selected to illustrate the regime of spiking-bursting oscillations at $\sigma = -0.25$ shown in Fig. 2(a). Arrows indicate the direction of switching between the branches in the case of (b).

When $\alpha > 4$ and the operating point is selected on $S_{pu}(y)$, then the phase of silence, corresponding to slow motion along $S_{ps}(y)$, and burst of spikes, when system moves along S_{spikes} , alternate. The burst of spikes begins when fixed points x_{ps} and x_{pu} merge together and disappear.

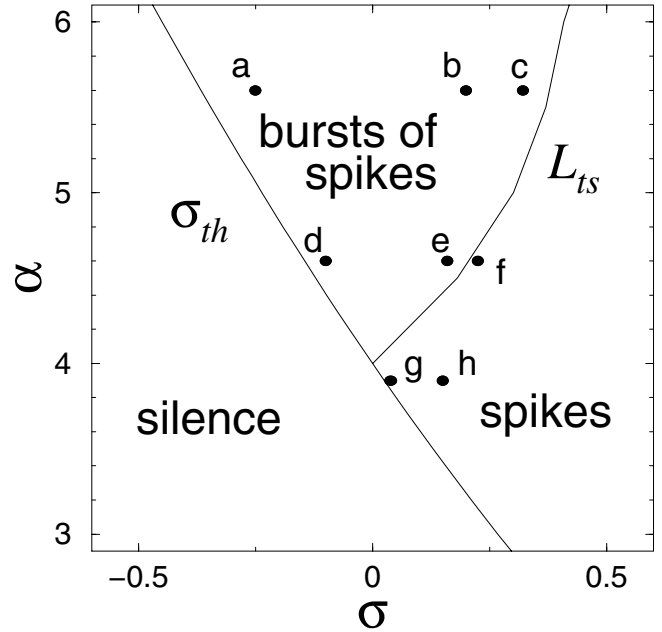


Fig. 4. Bifurcation diagram on the parameter plane (σ, α) . Dots in the diagram indicate the parameter values for the waveforms shown in Fig. 2. In a given scale bifurcation curve AH is undistinguishable from σ_{th} .

Before this state the system is in x_{ps} and, therefore, y increases. The termination of the burst happens when limit cycle P_k merges into homoclinic orbit h_{pu} and disappears. After that the fast subsystem flips to the stable fixed point x_{ps} and, then, the process repeats.

The results of the approximate analysis are summarized in the bifurcation diagram shown in Fig. 4. The bifurcation curve σ_{th} corresponds to the excitation threshold (4) where the map starts generating spikes. Curve L_{ts} shows the approximate location of the border between spiking and spiking-bursting regimes, obtained in the numerical simulations. Separation of spiking and bursting regimes is not always obvious, especially in the regime of chaotic spiking. The regime of spiking-bursting oscillations takes place within the upper triangle formed by curves σ_{th} and L_{ts} .

In the rest of the paper we will study the origin of chaotic oscillations which takes place in the vicinity of curves σ_{th} and L_{ts} . Chaos occurs due to interaction between the fast (1a) and slow (1b) maps, because each of these maps individually do not produce chaos. Therefore, the formation of chaotic behavior cannot be explained within the considered approximation $\mu \rightarrow 0$ and analysis of the two-dimensional dynamics of map (1) with finite values of μ is needed.

3. Fast and Slow Dynamics of 2D Map at Small Finite μ

To find the dynamical mechanisms behind the chaos onset we study (1) at finite small μ . We start with the stability analysis of the fixed point (OP) of the two-dimensional map and show how the finite values of μ alter the dynamics of the map near the bifurcation values where OP loses stability. Next we reveal the role of the special solutions — the so-called French canards in the chaotic dynamics of the map. We conclude the consideration by examining the bifurcations of homoclinic orbits associated with the repelling fixed point and their role in chaos formation.

3.1. Local bifurcation of the fixed point

We restrict our consideration to the rectangular $\{2 \leq a \leq 8; -2 \leq \sigma < 1\}$ in the parameter space. Within this rectangular, 2D map (1) has a single fixed point O with the coordinates $x_o = -1 + \sigma$, and $y_o = x_o - (\alpha/1 - x_o)$. Observe that as the value of σ becomes larger than 1 the fixed point disappears due to the discontinuity of function $f(x)$ in the interval $x > 0$, see (2).

Since O is a single fixed point within the given parameter domain a saddle-node bifurcation is impossible. Therefore, the analysis of the local codimension-1 bifurcations narrows to the Andronov–Hopf bifurcation, when the fixed point has a pair of multipliers equal to $e^{\pm i\psi}$, and the flip bifurcation where either multiplier equals -1 . Moreover, the last bifurcation can be excluded from our consideration. The arguments against this bifurcation are as follows: in the limit $\mu \rightarrow 0$ the fixed point at the threshold σ_{th} has two $+1$ multipliers, and hence, in virtue of continuity, the multipliers shall remain positive for all small μ .

The Jacobian matrix \mathbf{J} of the map at the fixed point is given by

$$\mathbf{J} = \begin{pmatrix} \frac{\alpha}{(2-\sigma)^2} & 1 \\ -\mu & 1 \end{pmatrix}.$$

In the case of the Andronov–Hopf (AH) bifurcation for maps the Jacobian and the trace of \mathbf{J} become 1 and $2 \cos \psi$, respectively. Then one can find the equation of bifurcation curve AH which is given by

$$\sigma = 2 - \sqrt{\alpha/(1-\mu)} \approx \sigma_{\text{th}}. \quad (6)$$

On curve AH the fixed point has the following multipliers:

$$\rho_{1,2} = \frac{2-\mu}{2} \pm \frac{i}{2} \sqrt{(4-\mu)\mu} = \cos \psi \pm i \sin \psi. \quad (7)$$

Observe that $\rho_{1,2}$ in (7) depend on μ only. The fixed point is attracting (repelling) on the left (right) of curve AH (σ_{th}) in the parameter plane, see Fig. 4. The stability of the fixed point on AH is determined by the sign of the first Lyapunov coefficient L_1 . The point is stable when $L_1 < 0$ and repelling otherwise. The tedious calculations of L_1 presented in Appendix reveal $L_1 > 0$. Therefore, the Andronov–Hopf bifurcation of the fixed point is *subcritical*.

3.2. Canards and chaotic spiking

The fact that the fixed point loses the stability through the Andronov–Hopf bifurcation alters essentially our picture of the behavior of map (1) near the threshold that was depicted in Sec. 2 in the limit $\mu \rightarrow 0$.

At the subcritical Andronov–Hopf bifurcation the fixed point loses its stability when an unstable invariant curve shrinks into it. To complete the picture of qualitative behavior of the map near the threshold we need to examine the evolution of this invariant curve with the parameter change, and answer the question: where does the unstable invariant curve come from? This analysis is straightforward if one can find the inverse of the map where this invariant curve becomes attractive. Despite our map (1) is noninvertible, nevertheless, locally in the domain $x \leq 0$ containing the fixed point the inverse is given by:

$$\begin{pmatrix} x \\ y \end{pmatrix} \mapsto \begin{pmatrix} Z \\ y + \mu(Z + 1 - \sigma) \end{pmatrix}, \quad (8)$$

with

$$Z = \frac{x - y + \mu\sigma - \sqrt{(x - y + \mu\sigma)^2 - 4\mu(x - y - \alpha - \mu(1 - \sigma))}}{2\mu}.$$

Having the above map one can now trace the invariant circle away from the Andronov–Hopf bifurcation back to its origin, and expect to observe any of its transformations.

A comprehensive answer to the question on the origin of the invariant curve requests an examination of a special solution known as a *canard* or a French duck. In the theory of dynamical systems

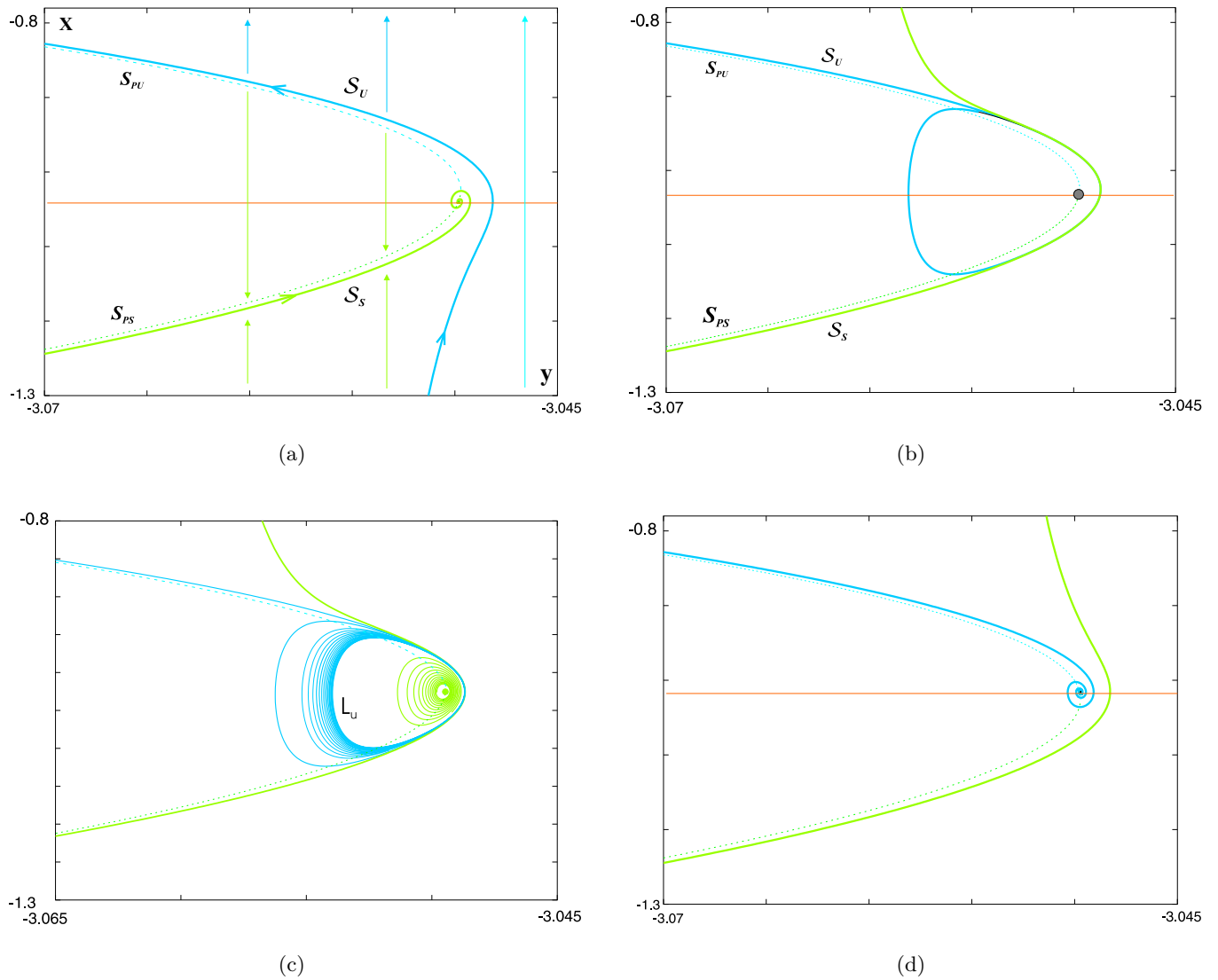


Fig. 5. Stages of canard formation: $\mu = 0.001$, $\alpha = 4.1$ and σ equal to (a) -0.0262 ; (b) -0.026113175787 ; (c) -0.02605 ; and (d) -0.016 . In panel (a) S_s converges to the stable point whose basin of attraction is determined by S_u . (b) Critical canard manifold and birth of the closed unstable invariant curve. (c) The last bounds the basin of the stable point. (d) The unstable critical manifold spirals out of the fixed point, stable in backward time.

with slow and fast variables this solution is quite typical near an excitation threshold [Diener, 1981; Eckhaus, 1983; Arnold *et al.*, 1994]. In our case we can also call it a Hopf-initiated canard for consistency with the classification proposed in [Guckenheimer *et al.*, 2000]. Based upon numerical simulations we will argue that the canard can cause chaos in the map near the subcritical Andronov–Hopf bifurcation for maps.

The mechanism underlying a canard can be reiterated in our case as follows. Consider the curve S_{fp} of slow motions of map (1) at $\mu = 0$. It consists of the two branches S_{ps} and S_{pu} corresponding

to the structurally stable attracting and repelling fixed points of the fast map respectively; see Figs. 3 and 5(a). The slow manifold lacks the normal hyperbolicity property near the fold where S_{ps} and S_{pu} merge; this fold is the saddle-node point of the fast map. As follows from [Fenichel, 1979] that when μ is small the normal hyperbolic pieces of S_{pu} and S_{ps} will persist as some invariant critical manifolds S_u and S_s , both μ -close to the original branches. As a control parameter of the system varies the manifolds S_u and S_s may touch each other, cross (in maps) thereby forming the canard manifold breaking up as they swap over in further.

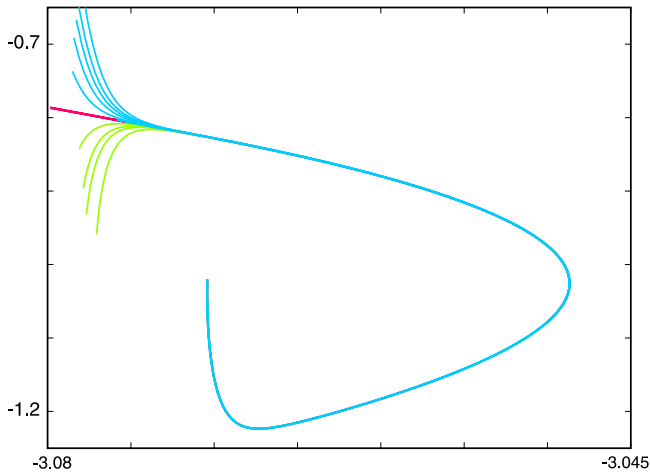


Fig. 6. Instability near the canard at $\alpha = 4.1$ and $\sigma = -0.026113175787$ broadcasts the initial interval of size 0.1^{-5} . The unstable critical manifold \mathcal{S}_u is shown in red.

Below we will illustrate numerically how the metamorphoses of these manifolds change the structure of the phase portrait of the map as the parameters α and σ vary. Prior to that we would like to sketch the algorithm used to compute the manifolds in the (x, y) -plane, considering the example of \mathcal{S}_s . A rather remote segment of the curve S_{ps} of slow motion is picked up as an initial approximation. Smallness of μ (throughout numerics we set $\mu = 0.001$ unless otherwise indicated) provides quick convergence of the chosen segment to \mathcal{S}_s whose further forward iterates trace out the location of the desired manifold. The smoothness of the manifold remains satisfactory even for relatively large (fast) values of μ provided the density of the points on the initial interval is high enough.

Four snapshots taking the critical manifolds near the fold are shown in Fig. 5 illustrating the evaluation of the canard as the parameter σ increases. In order to see the sequence of iterations generated by the map we connect the consecutive points of a trajectory in the phase plane. The first picture shows the stable critical manifold \mathcal{S}_s converging to the attracting fixed point before the Andronov–Hopf bifurcation. Figure 5(d) shows the unstable invariant manifold \mathcal{S}_u spiraling out of the now unstable fixed point after the bifurcation. When the bifurcation curve AH is crossed leftward, the fixed point becomes stable and its absorbing basin is bounded by the unstable invariant curve L_u . The latter is the α -limit set for the trajectories close to \mathcal{S}_u shown in Fig. 5(c). As σ decreases slightly further the size of L_u increases

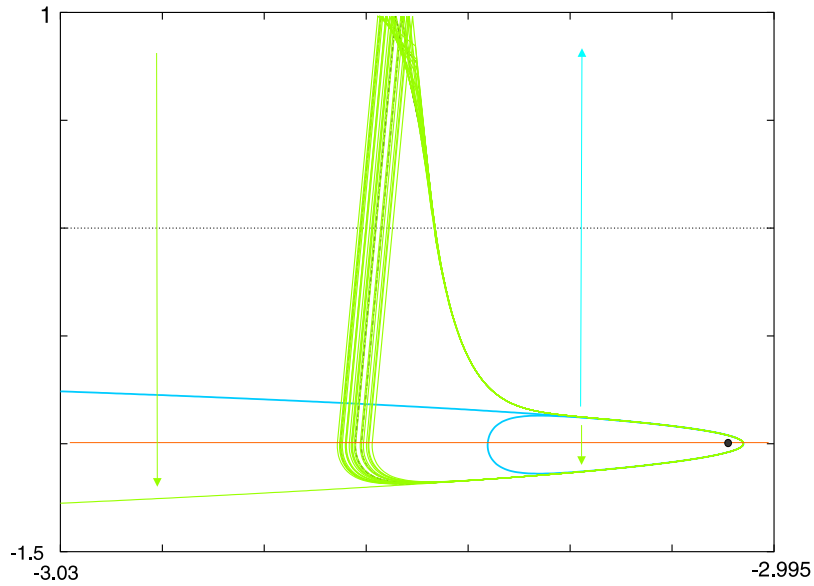
and at some critical value of σ the critical manifolds \mathcal{S}_s and \mathcal{S}_u touch each other, see Fig. 5(b). As they swap over each other, the invariant curve L_u vanishes, see Fig. 5(a).

The geometry of the critical manifolds suggests the numerical scheme for localizing the corresponding bifurcation curve in the (σ, α) -parameter plane. However, this curve is not presented in Fig. 4 because it is indiscernible from (i.e. $O(\mu)$ — close to) bifurcation curve AH (σ_{th}) on the scale adopted.

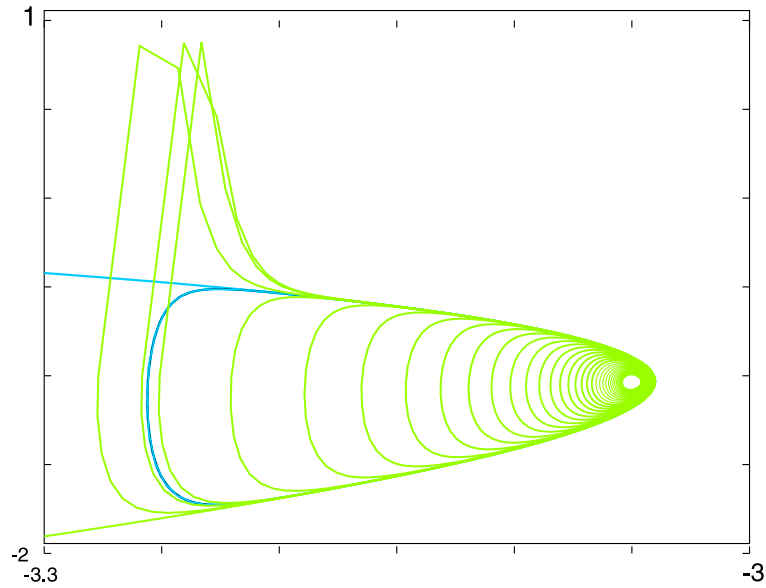
When the critical manifold \mathcal{S}_s moves further in parallel to \mathcal{S}_u a neighboring trajectory will be dragged along with it into the unstable region. Such a solution is called a *canard*. The canard solutions are characterized by a high sensitivity to initial conditions that is due to the blowing instability near the unstable critical manifold that separates and repels the nearby trajectories on both sides in opposite directions, see Fig. 6. When this instability lifts a trajectory up off the unstable critical line, it is mirrored by the limiter built in the function (2) downwards throughout line $x = -1$ towards stable critical manifold \mathcal{S}_s , along which the trajectory slides slowly to the right. Two distinct phase portraits reflecting this situation are shown in Fig. 7. Figure 7(a) illustrates the regime of bistability where the canard initiated chaos coexists with the stable fixed point whose local absorbing basin is surrounded by the unstable invariant closed curve L_u . Here, the beam of the phase trajectories first widens along the canard and then gets split and mixed at the point $(x = 0, y = \alpha)$ gluing the two piecewise continuous segments of nonlinear function (2) of the map (1). The chaotic attractor shown in Fig. 7(a) is the image of the continuous spiking characterized by irregular inter-spike-intervals. As one can see from the figure this type of spiking activity can coexist in the silent mode when the map is close enough to the threshold of excitation.

The canard bifurcation does not always lead to the appearance of the strange attractor in the map, and Fig. 7(b) evinces so showing that the unstable invariant curve no longer separates chaos from the basin of the stable fixed point. This corresponds to chaotic transitivity to the regime of silence.

To understand better the structure of chaos in 2D map (1) we introduce a 1D return mapping of an appropriate interval of the cross-section $x = \sigma - 1$, see Fig. 8. The following two images of this map shown in Fig. 9 for the same parameter values



(a)



(b)

Fig. 7. (a) Example of instant chaos at $\alpha = 3.995$, $\sigma = 0.0$ and $\mu = 0.001$. Due to spontaneous jumps of the phase point off the canard the number of its iterates as it climbs up the plateau on nonlinear characteristic differs for every circulation. (b) The unstable invariant curve does not bound the “local” attraction basin of the stable fixed point; $\alpha = 4.1$, $\sigma = -0.03445$ and $\mu = 0.00749915834$. By “local” the attraction basin of the stable fixed point of the locally invertible map is understood.

as in Fig. 7 reveal the structure of chaos in the original 2D map. The discontinuity points in the foliated region of the map are due to the gluing point separating eventually the orbits of any two close points. The pink point on the bisectrix is the image of the unstable critical manifold, and the middle

and the right one correspond to the unstable closed curve and the stable fixed point of the original map, respectively. It is clearly seen in Fig. 9(a) that in the case of the bistable regime the absorbing area of the stable fixed point and that of the strange attractor (containing no stable orbits if all slopes

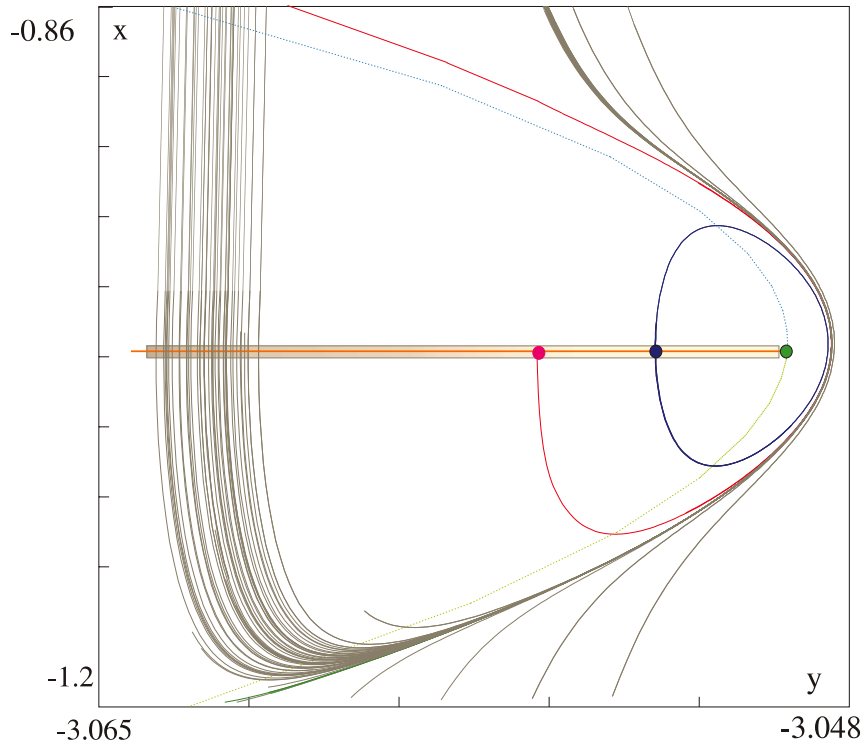


Fig. 8. Method for construction of one-dimensional return map ($y \rightarrow \bar{y}$). The return map is computed for the interval shown by a grey narrow rectangular. Shown are the closed unstable invariant curve (blue) and stable fixed point (green dot) which are, respectively, the unstable and stable fixed points in the 1D map presented in Fig. 9. The unstable critical line shown in red corresponds to the discontinuity gap in the 1D map.

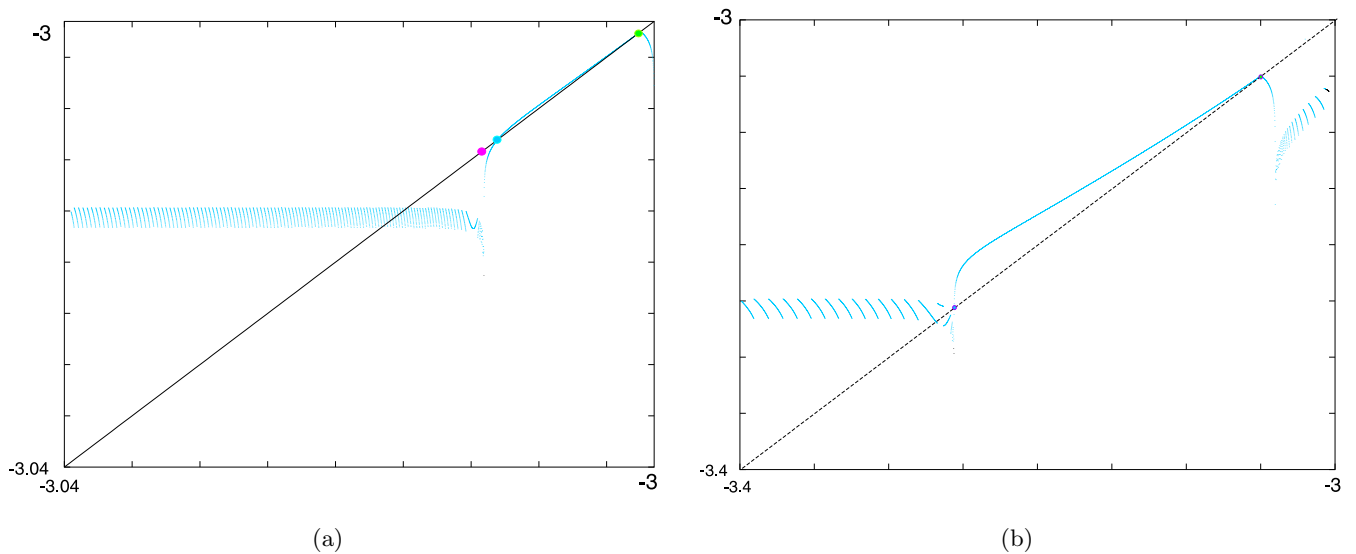
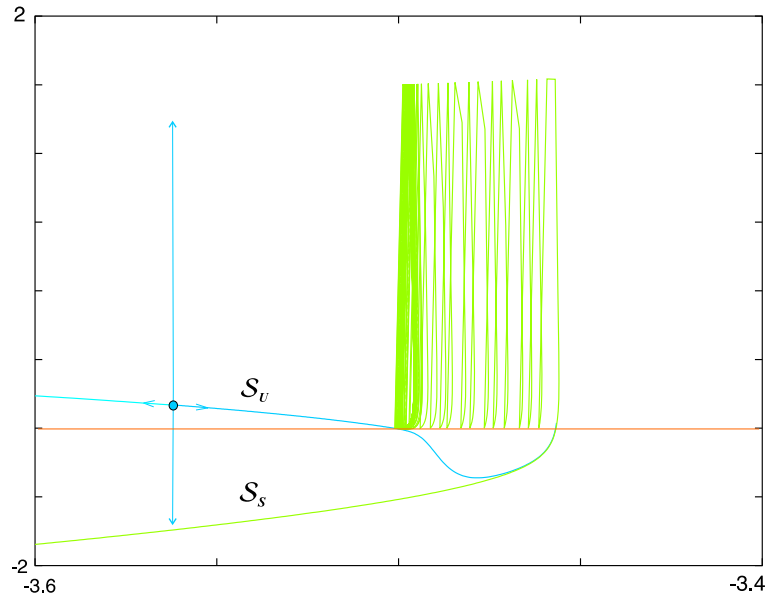
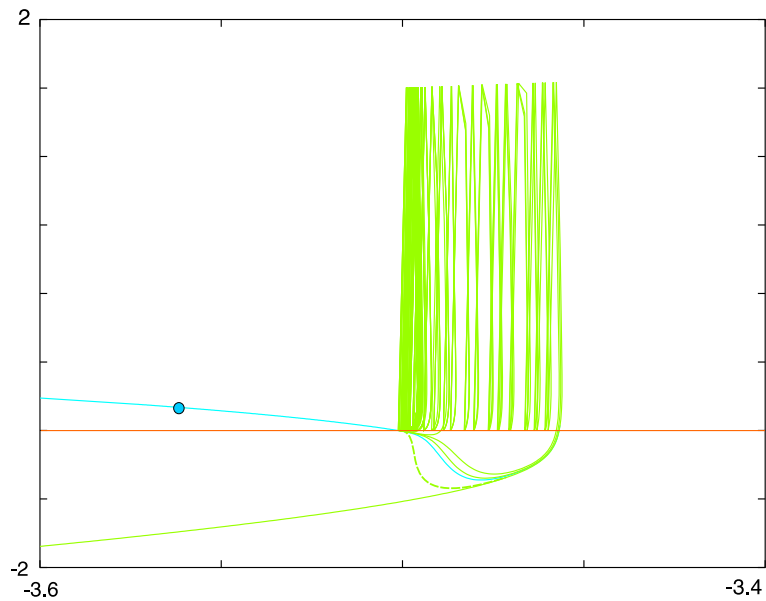


Fig. 9. One-dimensional return map ($y \rightarrow \bar{y}$) computed for the same parameter values as in Fig. 7. In (b) trajectories are thrown out of the region of chaos into the basin of the stable fixed point. Red point is the discontinuity point near the cross-section that is no longer global as the trajectories of the 2D map dragged along with the unstable critical lines do not return to the iterated interval. The blue and the green fixed points are the closed unstable invariant curve and the stable fixed point in the 2D map, respectively.



(a)



(b)

Fig. 10. Transformation of continuous spikes into bursts through the tangency of the stable and unstable critical lines. The bursting phase grows as the attractor goes beneath the unstable critical manifold. (a) $\alpha = 5$ and $\sigma = 0.3$; (b) $\sigma = 0.28$

of the zigzag portion of the graph are greater than one) do not overlap. This is not the case shown in Fig. 9(b) where the stable points are the only attractor in the map.

To conclude this section we resume that the canard initiated through the subcritical Andronov–Hopf bifurcation may cause the explosive transition from the silent phase to bursts with the irregular single spike in the narrow region ad-

joining to AH bifurcation curve in the parameter plane.

3.3. Chaotic bursting

The analysis of the map dynamics discussed in the previous subsection was focused on the onset of chaotic spiking activity near the threshold of excitation σ_{th} , see Fig. 4. In this section we will focus

on chaos origin at the transition from a continuous spiking to the bursts generation.

3.3.1. Transition from continuous spiking to bursts

Here we consider the transition from the regime of continuous spiking to the bursting activity that occurs within a wedge-shaped domain originating from the threshold ($\alpha = 4$; $\sigma = 0$). Note that these regimes are separated approximately in the parameter plane by curve L_{th} , see Fig. 4.

The mechanism of this transition in the case of finite values of μ is illustrated in Fig. 10. Green trajectory, whose initial point is chosen by the stable critical manifold \mathcal{S}_s , tends to same attractive ω -limit set. One can see that the map generates continuous spikes when the attractor is such as shown in Fig 10(a). In contrast, Fig. 10(b) illustrates the regime of bursts. Here a burst means that the continuous spiking phase is altered by relatively long interval of silence while the trajectory drifts along the stable critical manifold.

Consider the evolution of the shape of the attractor on the path ($\alpha = 5$; $\sigma = 0.3 \rightarrow 0.28$)

across this wedge-like region. Figure 10(a) is taken at $\sigma = 0.3$. At this moment the stable critical manifold \mathcal{S}_s makes a first touch with the unstable critical one \mathcal{S}_u at some point on the line $x = -1$. This situation is very similar to the canard formation discussed in Sec. 3.2. As then, the phase point can be dragged along the unstable critical manifold which results in a spontaneous jump up or down. This leads to high sensitivity of the trajectories' behavior on initial conditions and brings a chaotic component into the dynamics of bursts. As σ decreases further the attractor descends below \mathcal{S}_u so that the phase point makes straight jumps down onto the stable critical manifold, thereby forming a genuine burst in Fig. 10(b). The number of spikes in a burst can be constant or alternating depending on how close the attractor is to the unstable critical line.

The attractor of the continuous spiking activity presented in Fig. 10(a) appears in the phase portrait as a fuzzy object. To understand the dynamics of this continuous spiking we studied a bifurcation diagram for the transition from the regime of regular continuous spiking to the formation of the fuzzy object and then to the spiking-bursting regime. The

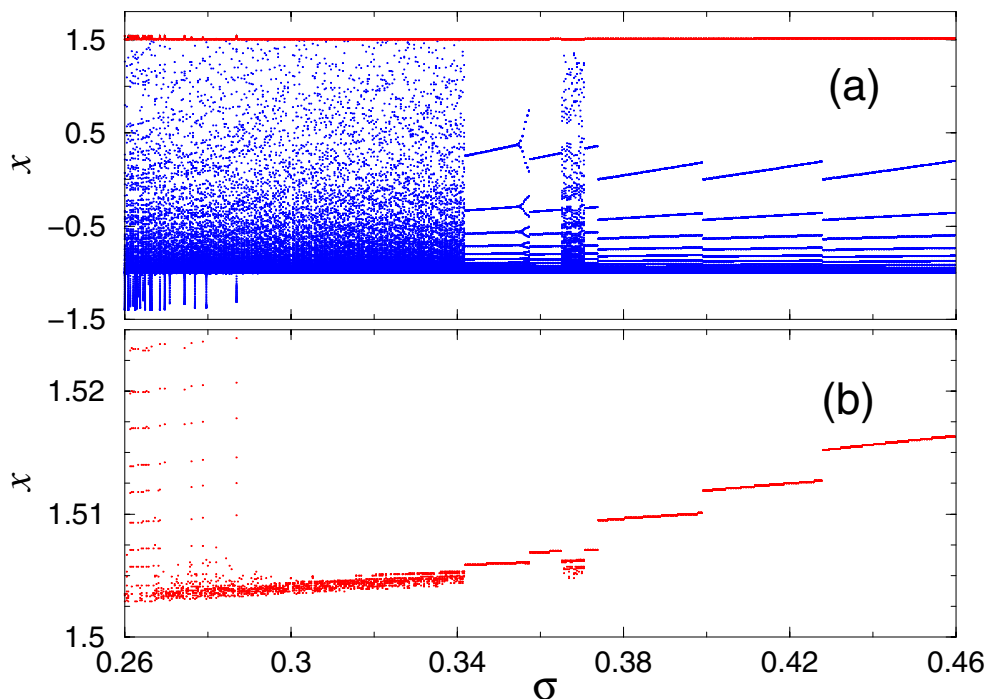


Fig. 11. Bifurcation diagram (σ, x_n) computed with $\alpha = 5$ illustrates the change of attractor in map (1) as the dynamics of the map transforms from the periodic to chaotic continuous spiking, and then to chaotic spiking-bursting behavior (a). Red dots in the diagram mark the iterations corresponding to the top of the spikes. Panel (b) shows a zoomed fragment of these “red” iterations where the values of x_n reflect the dynamics of slow variable y_n .

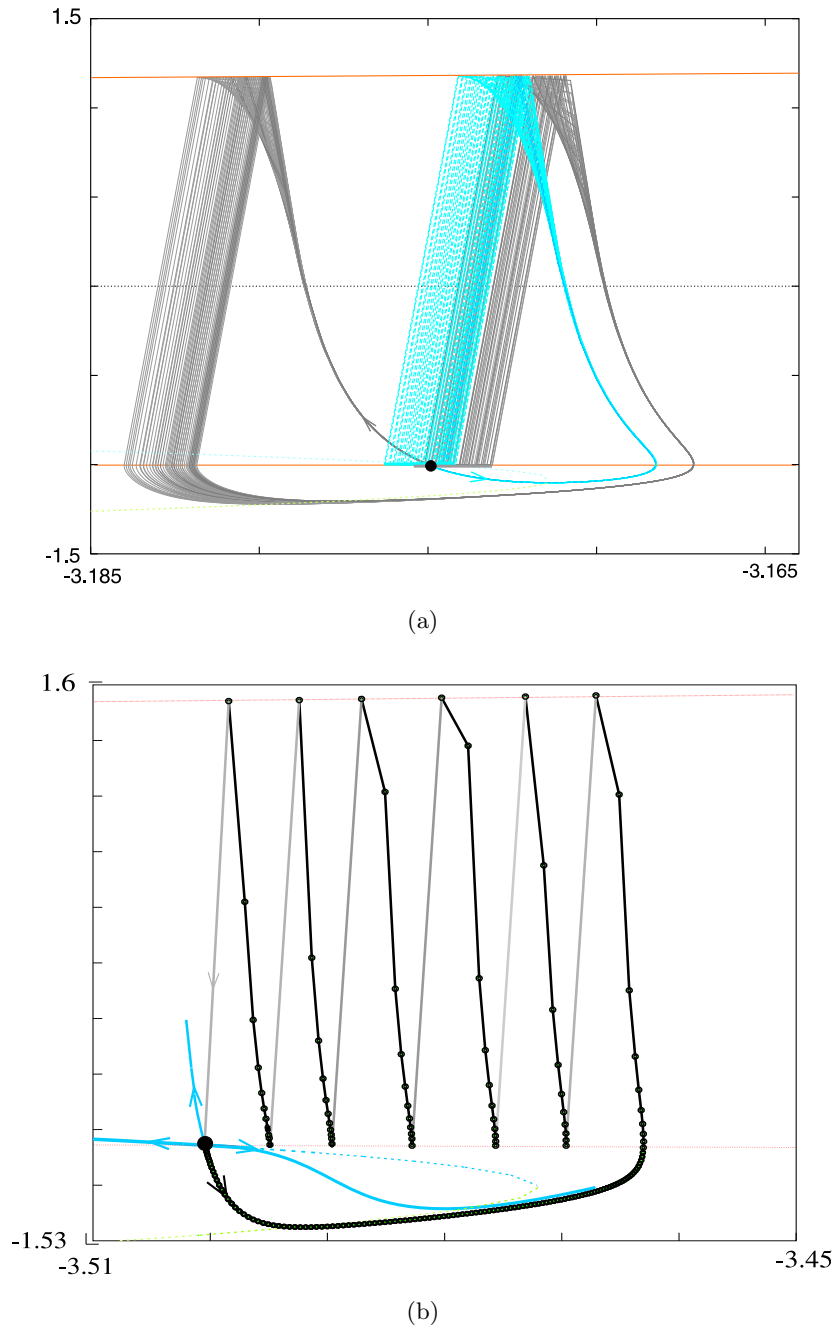


Fig. 12. (a) Primary homoclinics to the repelling point existing within $\alpha \in [4.3339; 4.3679]$ computed at $\alpha = 4.3499$; (b) shows the six-spike homoclinic orbit turning into a seven-spike one at $\alpha = 5.01$.

bifurcation diagram showing how the distribution of the points x_n of the attractors changes with σ is presented in Fig. 11(a). Note, that the points of the attractor forming a line on top of the diagram correspond to the moments of time when the map generates spikes. Therefore, as it follows from formula (2), $x_n = \alpha + y_n$, these points represent the values of y_n at the moment of each spike. The fragment of the bifurcation diagram that shows

this line of points in more detail is presented in Fig. 11(b).

One can clearly see from these diagrams that, before the transition to the spiking-bursting regime, the periodic spiking changes to the regime of chaotic continuous spiking. The spiking is periodic when the operating point (and, therefore, the attractor) is sufficiently far from the unstable critical curve. In this case there are no significant differences between

the dynamics of the limit cycles P_k with finite values of μ and with $\mu \rightarrow 0$. However, when the operating point gets close to the unstable critical curve the cycles P_k , which are superstable at $\mu = 0$, become unstable at finite values of μ . Due to this instability the slow variable, y_n , fluctuates and the trajectory wanders among various cycles P_k that coexist at the values of σ close to the critical one.

3.3.2. Homoclinic bifurcations of the repelling fixed point

This section discusses the mechanism of the generation of chaotic bursts via the homoclinic bifurcations of the repelling fixed point of the 2D map (1). Such a bifurcation is one of the features of noninvertible maps [Mira *et al.*, 1996]. In both invertible and noninvertible maps the existence of a homoclinic orbit is a key sign for the formation of complex, chaotic motions.

In our case the dimension of the unstable set W_O^u of the repelling fixed point O is two, whereas the stable set W_O^s is null-dimensional. The set W_{loc}^u is determined locally, near the fixed point where the inverse map (8) is defined. It consists of the points whose forward iterates under map (8) converge to the fixed point O . A point $p = W_O^u \cap W_O^s$ is a homoclinic one if its forward and backward iterates converge to the fixed point O . The fixed point is called a snap-back repeller if its small neighborhood contains a homoclinic point whose finite sequence of forward iterates ends up at the fixed point. A homoclinic orbit to the snap-back repeller can be transverse or not, depending on whether the forward images of W_{loc}^u cover the fixed point entirely or not. The existence of a transverse homoclinic orbit to the repeller implies the existence of a *scrambled set*, introduced by Marotto [1978]. The scrambled set is an analog of a hyperbolic subset which is the closure of the transverse homoclinic trajectory in a proper invertible map. It consists of countably many repelling periodic orbits and a continuum of positive Poisson stable trajectories. The presence of such trajectories is a signature of chaos [Shilnikov, 1997].

The existence of chaotic dynamics in map (1) could follow directly from Marotto's theorem if there were not one obstacle. In our map a homoclinic bifurcation may takes place only if the fixed point lies on $x = -1$, i.e. when $\sigma = 0$. This means that a homoclinic bifurcation in the map is of codimension-1.

Figure 12 shows the locus of the forward iterates of the points in W_{loc}^u starting with and landing onto line $x = -1$. If the original interval and its image on $x = -1$ both cover the fixed point, then the snap-back bifurcation is structurally stable in the α -parameter family. Moreover, the bifurcation takes place within a whole interval on the cut $\sigma = 0$ in the parameter plane.

The snap-back bifurcations and, respectively, the homoclinic orbits are distinguished by the number of spikes in a burst, see for example Fig. 12. In particular, Fig. 12(a) shows the map generating

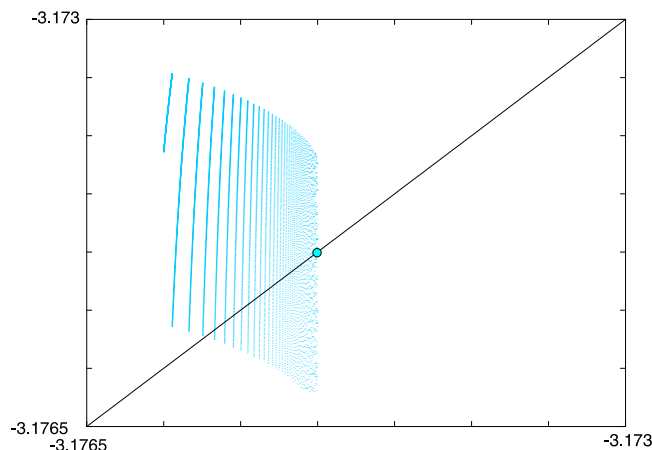


Fig. 13. 1D return map ($y \rightarrow \bar{y}$) computed for the interval on the cross-section $x = -1$. The shape of the map indicates that the homoclinic orbit is structurally stable in α -parameter cut; $\alpha = 4.3499$, $\sigma = 0$ and $\mu = 0.001$.

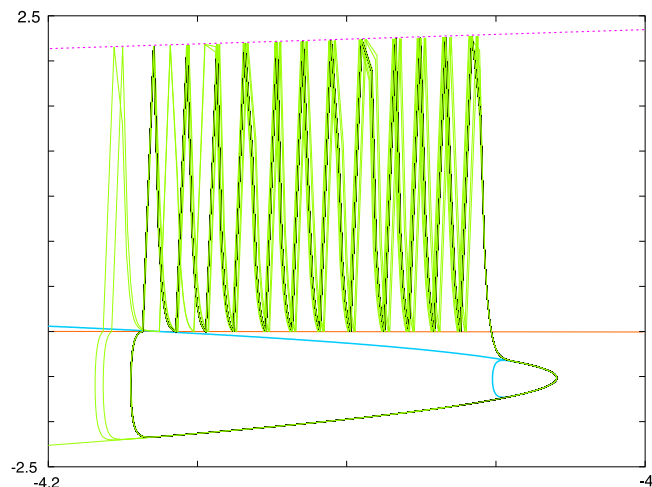


Fig. 14. Canards computed with $\alpha = 6.30749986$ and $\sigma = -0.513045789$. The trajectory (green) goes along the unstable manifold S_u (shown in blue) at two locations. First one is at the beginning of the burst (on the right-hand side) and, the second is at the end of the burst (on the left-hand side).

chaotic sequences of the single and the double-pulse bursts.

Another computer assisted way of proving the chaotic dynamics in the map near the snap-back repeller relies on the analysis of a one-dimensional return map of a segment on $x = -1$. This map is shown in Fig. 13 at $\alpha = 4.345$. The interval under consideration is of size $\sim 10^{-5}$ whose right end point is the snap-back repeller. One can see that the map at the indicated parameter values is expansion. The points of intersections of the graph of the map and the bisectrix correspond to the unstable periodic orbits of distinct periods. Moreover, since the fixed point is in the range of the map whose graph has a foliated structure, this suggests the existence of infinitely many homoclinic orbits accumulating to the primary one. The last ones and the periodic points form a skeleton of a chaotic set which can be an attractor of the map generating the bursts with irregular numbers of spikes.

Another, yet similar, way of waveform transformations is illustrated in Fig. 14 far from the homoclinic bifurcation. As above, the core of the mechanism is the interplay between the unstable manifold \mathcal{S}_u and the locus of the attractor. Recall that the direction of the jump — up or down of the phase point landing onto the line $x = -1$ is determined whether its coordinates are above or below \mathcal{S}_u respectively. However, it may happen that the point passes close by the intersection point of \mathcal{S}_u and $x = -1$. Then it results in some successive iterates of the phase point running closely along \mathcal{S}_u until an accumulative sharp jump up or down. It is evident that the duration and the length of such canardic phase depends on how close the phase point was picked up or turns out intermediately to be next to \mathcal{S}_u .

4. Conclusion

Our bifurcation analysis reveals the origin of chaotic behavior of a simple two-dimensional discrete-time model of spiking-bursting neural activity. The model consists of fast and slow subsystems coupled to each other. The individual dynamics of the fast subsystem is characterized by existence of bistable regime, where a superstable limit cycle, corresponding to the spike generation, and a stable fixed point, corresponding to the silence, coexist. When this subsystem is coupled with the slow subsystem that has neutral individual stability the whole system becomes capable of generating chaotic spiking and spiking-bursting activity.

We have shown that the instability of trajectories needed for onset of chaos generation occurs due to the formation of canard solutions or due to motions near a snap-back repeller. The canard solutions are quite typical near the excitation threshold and the transition between continuous spiking and spiking-bursting behavior. The dynamics near snap-back repeller can occur in the spiking-bursting regime.

The instability itself is not sufficient to guarantee the chaotic behavior. A very important component of chaos in this map is the time discretization. Sharp changes of the period of spiking in our discrete-time model provides mixing which is a necessary element in the formation of a chaotic set. Although the discretization of time is not an attribute of complex dynamics of biological neurons this discrete-time model captures the onset of chaotic spiking-bursting behavior in real neurons quite well. Chaotic component in the model behavior caused by the discrete-timing can be treated here as the influence of complex high-dimensional dynamics of ionic currents and/or as a stochastic component of ionic channels which bring irregularity to the spiking-bursting neural activity.

The canard transitions (safe and dangerous) in this and similar maps that we have analyzed so far give rise to a number of curious problems related to the general theory of continuous and discrete French ducks as well as the relative numerical species. One of these is whether the stable and unstable critical canard manifolds may cross in a way that stable and unstable separatrices of a saddle point in a 2D diffeomorphism do, and if it is so, what size of the wriggles is, i.e. $\sim e^{-\frac{1}{\mu}}$ or the crossings may be super-exponentially small $\sim e^{-\frac{1}{e^{-\frac{1}{\mu}}}}$ as conjectured by [Gelfreich & Turaev, 2002]. A comprehensive answer is to engage the extremely precise computations that are beyond the scope of the given study. Nevertheless, all our persistent attempts to detect the crossing numerically using double precision have failed. Another related issue is a tremendous sensibility of the orbits of the map near the canard threshold where infinitesimal (in terms of computer precision, i.e. 10^{12-13}) changes in parameter values imply significant qualitative and quantitative alterations in the behavior of the supposedly trivial solutions of the slow-fast maps, see Fig. 15. So, this intriguing problem is yet to open and to be understood.

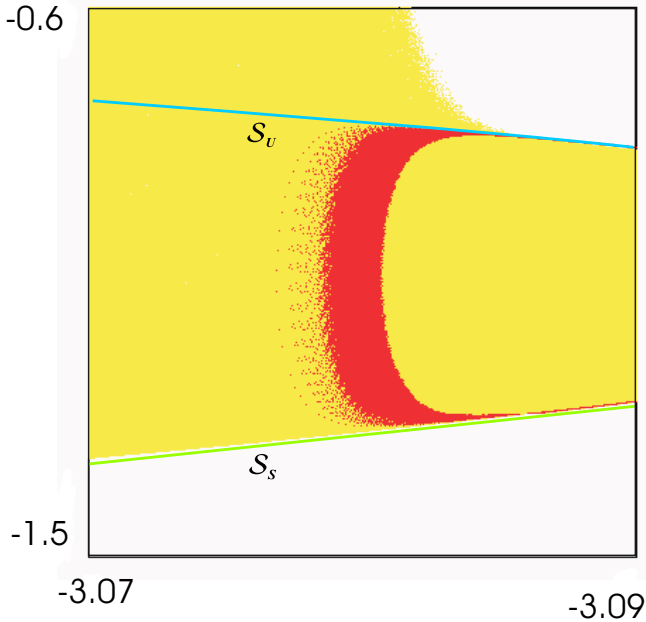


Fig. 15. Disintegration of the unstable invariant curve L_u into a nontrivial set (red dots) at $\alpha = 4.1$, $\mu = 0.001$ and $\sigma = -0.0261131991686799$. The attraction basing of “former” L_u in the backward time is shown in yellow. The visual fractal thickness of the invariant curve (red) suggest a conjecture that the breakdown of the curve is accompanied by the formation of the heteroclinic wiggles (crossing) of the stable and unstable manifolds \mathcal{S}_s and \mathcal{S}_u . Courtesy of C. Mira.

Acknowledgments

We would like to thank Dima Turaev and Christian Mira for useful discussions, especially, about issues related to the fine structure of the canards in the dynamics of maps. N. Rulkov was supported in part by U.S. Department of Energy (grant DE-FG03-95ER14516).

References

- Abarbanel, H. D. I., Rabinovich, M. I., Selverston, A., Bazhenov, M. V., Huerta, R., Sushchik, M. & Rubchinskii, L. [1996] “Synchronization in neural networks,” *Physics-Uspekhi* **39**, 337–362.
- Arnold, V. I., Afrajmovich, V. S., Ilyashenko, Yu. S. & Shilnikov, L. P. [1994] “Bifurcation theory,” *Dynamical Systems*, Encyclopaedia of Mathematical Sciences V (Springer-Verlag).
- Belykh, V. N., Belykh, I. V., Colding-Joregensen, M. & Mosekilde, E. [2000] “Homoclinic bifurcations leading to the emergence of bursting oscillations in cell model,” *Eur. Phys. J.* **E3**, 205–219.
- Buchholtz, F., Golowash, J., Epstain, I. R. & Marder, E. [1992] “Mathematical-model of an identified stomatogastric ganglion neuron,” *J. Neurophysiol.* **67**, 332–340.
- Chay, T. R. [1985] “Chaos in a three-variable model of an excitable cell,” *Physica* **D16**, 233–242.
- Chay, T. R. [1990] “Electrical bursting and intracellular Ca^{2+} oscillations in excitable cell models,” *Biol. Cybern.* **63**, 15–23.
- Chay, T. R., Fan, Y. S. & Lee, Y. S. [1995] “Bursting, spiking, chaos, fractals, and universality in biological rhythms,” *Int. J. Bifurcation and Chaos* **5**, 595–635.
- Diener, M. [1981] “Canards et bifurcations,” in *Mathematical Tools and Models for Control, Systems Analysis and Signal Processing*, Vol. 3, CNRS (Toulouse/Paris), pp. 289–313.
- Eckhaus, W. [1983] *A Standard Chase on French Ducks*, Lecture Notes in Mathematics, Vol. 985, pp. 449–494.
- Fenichel, N. [1979] “Geometric singular perturbation theory,” *J. Diff. Eq.* **31**, 53–98.
- Gelfreich, V. & Turaev, D. [2002] verbal communication.
- Golomb, D., Guckenheimer, J. & Gueron, S. [1993] “Reduction of a channel-based model for a stomatogastric ganglion LP neuron,” *Biol. Cybern.* **69**, 129–137.
- Guckenheimer, J., Hoffman, K. & Weckesserand, W. [2000] “Numerical computations of canards,” *Int. J. Bifurcation and Chaos* **2**, 2669–2689.
- Hindmarsh, J. L. & Rose, R. M. [1984] “A model of neuronal bursting using 3 coupled 1st order differential-equations,” *Proc. R. Soc. London* **B221**(1222), 87–102.
- Hodgkin, A. L. & Huxley, A. F. [1952] “A quantitative description of membrane current and its application to conduction and excitation in nerve,” *J. Physiol.* **117**, 500–544.
- Izhikevich, E. M. [2000] “Neural excitability, spiking and bursting,” *Int. J. Bifurcation and Chaos* **10**, 1171–1266.
- Marotto, J.R. [1978] “Snap-back repeller implies chaos in R^n ,” *J. Math. Anal. Appl.* **63**, 199–223.
- Mira, C., Gardini, L., Barugola, A. & Cathala, J.-C. [1996] *Chaotic Dynamics in Two-Dimensional Noninvertible Maps* (World Scientific, Singapore).
- Rinzel, J. [1985] “Bursting oscillations in an excitable membrane model,” *Ordinary and Partial Differential Equations*, eds. Sleeman, B. D. & Jarvis, R. J., Lecture Notes in Mathematics, Vol. 1151 (Springer, NY), pp. 304–316.
- Rinzel, J. [1987] “A formal classification of bursting mechanisms in excitable systems,” in *Mathematical Topics in Population Biology, Morphogenesis, and Neurosciences*, eds. Teramoto, E. & Yamaguti, M., Lecture Notes in Biomathematics, Vol. 71 (Springer, NY), pp. 267–281.
- Rulkov, N. F. [2002] “Modeling of spiking-bursting neural behavior using two-dimensional map,” *Phys. Rev.* **E65**, 041922.
- Shilnikov, L. P. [1997] “Mathematical problems of nonlinear dynamics: A tutorial,” *Int. J. Bifurcation and Chaos* **7**, 1953–2003.

Shilnikov, L. P., Shilnikov, A. L., Turaev, D. V. & Chua, L. O. [2001] *Methods of Qualitative Theory for Nonlinear Dynamics, Part II* (World Scientific, Singapore).

Wang, X.-J. [1993] "Genesis of bursting oscillations in the Hindmarch-Rose model and homoclinicity to a chaotic saddle," *Physica* **D62**, 263–274.

Appendix

The First Lyapunov Value L_1

Here we present the calculations of the first Lyapunov value at the fixed point at the Andronov–Hopf bifurcation. The consideration is reduced to the stability analysis of the critical fixed point of the local map:

$$\bar{x} = \frac{\alpha}{1-x} + y, \tag{A.1a}$$

$$\bar{y} = y - \mu(x + 1 - \sigma). \tag{A.1b}$$

Let us translate the fixed point to the origin by applying the transformation

$$\begin{pmatrix} x \\ y \end{pmatrix} \mapsto \begin{pmatrix} x + \sigma - 1 \\ y + \sigma - 1 - \frac{\alpha}{2 - \sigma} \end{pmatrix}.$$

Next we express the right-hand side of (A.1a) as the Taylor polynomial; only first three terms will be needed:

$$\begin{aligned} \bar{x} &= y + \frac{\alpha}{(2 - \sigma)^2}x + \frac{\alpha}{(2 - \sigma)^3}x^2 \\ &\quad + \frac{\alpha}{(2 - \sigma)^4}x^3 + O(x^4), \\ \bar{y} &= y - \mu x. \end{aligned} \tag{A.2}$$

Applying the coordinate transformation

$$\begin{pmatrix} x \\ y \end{pmatrix} \mapsto \begin{pmatrix} 0 & 1 \\ \sin \psi & -1 \cos \psi + \mu \end{pmatrix} \begin{pmatrix} \xi \\ \eta \end{pmatrix}$$

makes the linear part of (A.2) a rotation through the angle ψ :

$$\begin{aligned} \begin{pmatrix} \bar{\xi} \\ \bar{\eta} \end{pmatrix} &= \begin{pmatrix} \cos \psi & -\sin \psi \\ \sin \psi & \cos \psi \end{pmatrix} \begin{pmatrix} \xi \\ \eta \end{pmatrix} \\ &\quad + \begin{pmatrix} 0 \\ \frac{\alpha}{(2 - \sigma)^3}\eta^2 + \frac{\alpha}{(2 - \sigma)^4}\eta^3 + O(\eta^4) \end{pmatrix}. \end{aligned}$$

Having introduced $z = \xi + i\eta$, the map recasts in the complex form

$$\begin{aligned} \bar{z} &= ze^{i\psi} + i \left(-\frac{\alpha(z - z^*)^2}{4(2 - \sigma)^3} + i\frac{\alpha(z - z^*)^3}{8(2 - \sigma)^4} \right) \\ &\quad + O(|z|^4), \end{aligned}$$

where z^* is the z -conjugate. As follows from [Shilnikov *et al.*, 2001], the quadratic terms

$$\bar{z} = ze^{i\psi} + \frac{c_{20}}{2}z^2 + c_{11}zz^* + \frac{c_{02}}{2}z^{*2} + O(|z|^3)$$

with

$$\begin{aligned} c_{20} &= -\frac{i\alpha}{2(2 - \sigma)^3}, & c_{11} &= \frac{i\alpha}{2(2 - \sigma)^3}, \\ c_{02} &= -\frac{i\alpha}{2(2 - \sigma)^3}, \end{aligned} \tag{A.3}$$

are eliminated by the normalizing transformation

$$z \mapsto z - \frac{c_{20}}{e^{2i\psi} - e^{i\psi}}z^2 - \frac{c_{11}}{1 - e^{i\psi}}zz^* - \frac{c_{02}}{e^{-2i\psi} - e^{i\psi}}z^{*2}.$$

The resulting normal form finally assumes the canonical form:

$$z = e^{i\psi} + L_1z^2z^* + O(|z|^3),$$

where $O(|z|^3)$ denotes the remaining cubic and higher order terms. The expression for the first Lyapunov value reads as follows:

$$\begin{aligned} L_1 &= -\operatorname{Re} \left[\frac{e^{-i\psi}c_{21}}{2} \right] + \operatorname{Re} \frac{(1 - 2e^{i\psi})e^{-2i\psi}c_{20}c_{11}}{2(1 - e^{i\psi})} \\ &\quad + \frac{|c_{11}|^2}{2} + \frac{|c_{02}|^2}{4}. \end{aligned} \tag{A.4}$$

Plugging (A.3) into (A.4) yields

$$L_1 = \frac{(2 - \mu)(1 - \mu)(4 - 2\mu + \mu^2)}{16(2 - \sigma)^2}. \tag{A.5}$$

One can see $L_1 > 0$ when μ is small.

Note that as follows from [Arnold *et al.*, 1994] the sign of L_1 might be estimated as $\partial^3 \bar{x} / \partial x^3$ from (A.2) at $\sigma = 0$ and $\alpha = 4$. This is in agreement with (A.5).